

Measurement of Ultrashort Biphoton Correlation Times with an Integrated Two-Color Broadband SU(1, 1)-Interferometer

F. Roeder[✉], R. Pollmann[✉], M. Stefszky[✉], M. Santandrea, K.-H. Luo[✉], V. Quiring, R. Ricken, C. Eigner[✉], B. Brecht[✉], and C. Silberhorn[✉]

Paderborn University, Department of Physics, Integrated Quantum Optics, Institute for Photonic Quantum Systems (PhoQS), Warburger Straße 100, Paderborn 33098, Germany



(Received 5 November 2023; revised 14 December 2023; accepted 1 May 2024; published 31 May 2024)

The biphoton correlation time, a measure for the conditional uncertainty in the temporal arrival of two photons from a photon pair source, is a key performance identifier for many quantum spectroscopy applications, with shorter correlation times typically yielding better performance. Furthermore, it provides fundamental insight into the effects of dispersion on the biphoton state. Here, we show that a characteristic dependence of the width of the temporal interferogram can be exploited to obtain insights into the amount of second-order dispersion inside the interferometer and to retrieve actual and Fourier-limited ultrashort biphoton correlation times of around 100 fs. In the presented scheme, we simultaneously measure spectral and temporal interferograms at the output of an SU(1, 1) interferometer based on an integrated broadband parametric down-conversion source in a Ti:LiNbO₃ waveguide.

DOI: 10.1103/PRXQuantum.5.020350

I. INTRODUCTION

Quantum spectroscopy has raised significant interest as a tool for the investigation of materials and light-sensitive biological samples at the single-photon level [1–6]. In classical spectroscopy, linear interferometers are widely used to estimate the phase properties of a system under test, e.g., in spectral phase interferometry, direct field reconstruction, or linear interference [7,8]. An alternative system is the use of nonlinear interferometers, also called SU(1, 1) interferometers, that contain active optical elements and thereby provide different mechanisms of phase detection compared to linear interferometers [9–12]. These interferometers have attracted much attention as it is possible to achieve superior phase sensitivity with them [13–15]. Introducing tailored spectral phases inside the interferometer ultimately even allows for shaping of the quantum state at the output of the interferometer [16–18]. In addition, SU(1, 1) interferometry allows for operating the different interferometric paths with different colors. This has enabled various protocols of quantum metrology, such as spectroscopy, imaging, or optical coherence tomography with undetected photons; these are of particular interest for life science experiments [19–27] because they separate the

detected wavelength from the probe light and remove the need for detecting light at unfavorable wavelengths such as in the midinfrared.

The realization of these measurement concepts raises the need for bright and broadband biphoton sources that generate strong time-frequency entanglement. A high source brightness is typically achieved with integrated optics solutions that offer long interaction lengths and tight field confinement. Broadband operation then requires a careful engineering of the waveguide dispersion [28]. Strong time-frequency entanglement, finally, is characterized by the product of the biphoton correlation bandwidth—in typical cases and in this paper the linewidth of a continuous-wave pump laser—and the biphoton correlation time. The latter generally limits the performance of quantum spectroscopy by limiting achievable resolutions. Furthermore, the correlation time provides fundamental insights into the effects of dispersion on the broadband biphoton [29–34], which becomes even more critical for waveguide sources that may introduce significant amounts of dispersion during propagation.

As the correlation times of broadband sources are typically of the order of 10–100 fs, they are hard to measure due to insufficient detector timing resolution. Classical characterization techniques for ultrashort pulses, e.g., FROG or SPIDER, rely on nonlinear interactions that require high intensities and are therefore not applicable to single photons [7,8], while methods based on single-photon interferometry typically require coincidence detection and do not capture dispersive effects [35]. Recent development in these interferometers have however shown

*Corresponding author: franz.roeder@uni-paderborn.de

Published by the American Physical Society under the terms of the [Creative Commons Attribution 4.0 International license](#). Further distribution of this work must maintain attribution to the author(s) and the published article's title, journal citation, and DOI.

that second-order dispersion can be sensed in asymmetric designs or by utilizing the photon's temporal mode structure [36–38]. Methods based on nonlinear interactions are limited in resolution by the duration of a strong gating pulse [39], which is especially limiting for emerging nondegenerate broadband biphoton sources [34,40–43] with even shorter correlation times than that of the source used here. Therefore, a new scheme for measuring the correlation time of single-photon sources is required that also allows characterization at highly nondegenerate wavelengths.

Here we introduce a new technique to measure the correlation time of a broadband, integrated biphoton source that can be measured by incorporating the source into an SU (1, 1)-interferometer. We generate biphotons via parametric down-conversion (PDC) in a dispersion-engineered, periodically poled titanium-indiffused waveguide in lithium niobate. We note that the concepts in this work equally apply to photon pair sources based on four-wave mixing, although we focus on PDC. In the experiment, we observe a characteristic dependence of the width of the temporal interferograms for varying amounts of second-order dispersion inside the interferometer. Furthermore, we show that the observed characteristic dependence is affected by the spectral shape of the PDC source. We develop a supporting theory, which allows us to find a functional dependence between temporal and spectral measurements and to extract the Fourier-limited correlation time. This finding allows us to characterize other sources for optimal operation of the interferometer as this information is key for further applications, e.g., entangled two-photon absorption where knowledge about the biphoton correlation time is a crucial parameter for correctly retrieving the absorption cross section.

II. CONCEPT

The biphoton state from the photon pair generation process in a nonlinear material can be written as $|\psi\rangle_{\text{PDC}} = \int d\omega_s d\omega_i f(\omega_s, \omega_i) |\omega_s, \omega_i\rangle = \int d\tau_s d\tau_i \tilde{f}(\tau_s, \tau_i) |\tau_s, \tau_i\rangle$ with the transformations between the frequency and time domains given in Appendix A. It is described via the joint spectral amplitude (JSA) $f(\omega_s, \omega_i)$ in the frequency domain, which contains information about time-frequency entanglement between signal and idler photons $\omega_{s,i}$ in a generated state. In the temporal domain, the joint temporal amplitude (JTA) $\tilde{f}(\tau_s, \tau_i)$ is connected to the JSA via Fourier transform and contains information about the correlation time as the uncertainty in signal and idler arrival times $\tau_{s,i}$ [44,45]. The joint spectral intensity (JSI), the modulus square of the JSA, of a broadband PDC can be directly measured with established methods [46]. However, the joint temporal intensity (JTI), the modulus square of the JTA, and thereby the biphoton correlation time, defined as the FWHM of the JTI [28], is hard to measure directly

[47]. Furthermore, it cannot generally be retrieved from a Fourier transform of the JSI; a possible complex phase on the JSA whose information gets lost when measuring the JSI can lead to an increased correlation time and associated broadening of the JTA and thus, consequently, the JTI, as schematically shown in Fig. 1(a).

In our measurement concept, shown in Fig. 1(b), we build an SU (1, 1) interferometer from two identical biphoton sources—in our case a PDC source in a double pass configuration detailed later—and record temporal interferograms observed by counting signal and idler photons at the output of the interferometer when introducing a relative temporal delay between the two photons. We show that the correlation time of the biphoton can be determined by monitoring the width of these interferograms as the amount of second-order dispersion in the interferometer is varied, as depicted in the inset of Fig. 1(d).

By varying the spectral envelope of the generated PDC shown in Fig. 1(c) and observing the FWHM of the temporal interferogram, we note different characteristic dependencies. From this behavior we can extract the minimal, that is, the Fourier-limited, correlation time of the biphoton as well as the actual correlation time that is subject to the material dispersion of the source for different source operating conditions; see Fig. 1(d).

Our method is based on a model of an SU (1, 1) interferometer including a broadband PDC process. For this, we start from the JSA of a single PDC waveguide pumped by a cw laser, which is given by [44]

$$f(\Delta\omega) = \text{sinc}\left(\frac{\Delta\beta(\Delta\omega)L}{2}\right)e^{i\Delta\beta(\Delta\omega)L/2}, \quad (1)$$

where $\Delta\omega = \omega_s - \bar{\omega}_s = -(\omega_i - \bar{\omega}_i)$ is the frequency detuning from the central signal frequency $\bar{\omega}_s$, L is the length of the waveguide, and $\Delta\beta$ is the phase mismatch between the pump and the generated signal and idler fields. The exponential term in this expression contains the phase caused by the dispersion of the waveguide.

Achieving the desired short correlation times requires the production of a broad biphoton spectrum. Long waveguides typically generate narrow biphoton spectra, especially in the case of two color sources. Therefore, we use dispersion engineering to achieve a PDC source where signal and idler group velocities are matched to generate broader spectra. If we now expand $\Delta\beta$ up to second order [48] and make use of the strong frequency correlations due to cw pumping, we arrive at a phase mismatch $\Delta\beta$ that only shows quadratic terms in $\Delta\omega$ to leading order, as presented in Appendix A. With this, the JSA can be written as

$$f(\Delta\omega) = \text{sinc}(\Delta\gamma\Delta\omega^2)e^{i(\Delta\gamma\Delta\omega^2)}. \quad (2)$$

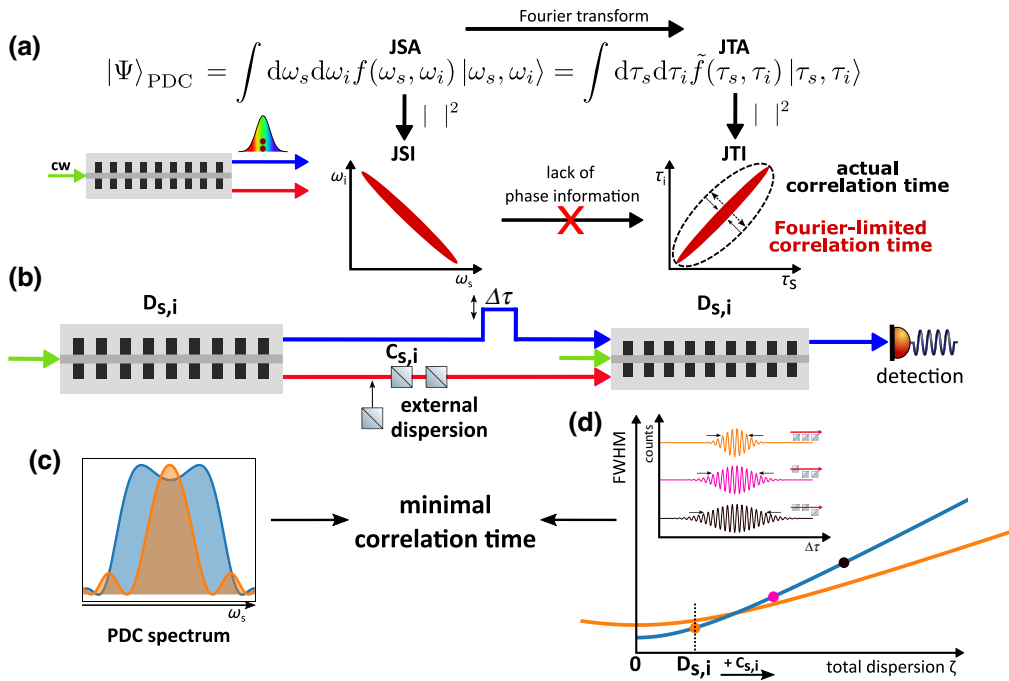


FIG. 1. (a) For a given PDC state of a broadband biphoton source, described by the JSA in the spectral domain and the JTA in the temporal domain, the directly measurable JSI does not allow one to retrieve the JTI due to a lack of phase information. The JTI might therefore be broadened due to second-order dispersion. (b) Incorporating a broadband PDC source in an SU (1, 1) interferometer allows one to extract the correlation time for different PDC spectra by measuring the characteristic dependence of the temporal interference width for different amounts of total second-order dispersion in the interferometer. This contains the intrinsic waveguide dispersion for the signal and idler photons, $D_{s,i}$, and an additional external dispersion, $C_{s,i}$. (c) Two signal spectra from the PDC source can be realized at different operating temperatures. They exhibit different spectral envelopes and widths and therefore different Fourier-limited correlation times. (d) The correlation time of the biphoton can be determined by monitoring the width of the temporal interferograms as the amount of second-order dispersion in the interferometer, consisting of internal waveguide dispersion $D_{s,i}$ and externally applied dispersion $C_{s,i}$, is varied, as depicted in the inset.

It becomes apparent that the group delay dispersion associated with the waveguide $\Delta\gamma = -[(D_s + D_i)L]/2$, including the second-order dispersion of signal D_s and idler D_i , defines the bandwidth of the JSA in this approximation. Combining two of our PDC sources in the interferometer and including a phase between them yields a total joint spectral amplitude of the whole interferometer $f_{\text{SU}(1,1)}(\Delta\omega)$. This expression includes a phase caused by the intrinsic second-order dispersion from the waveguide $(D_s + D_i)L\Delta\omega^2$ and an externally applied phase $\Phi_{\text{ext}}(\Delta\omega)$ (cf. Appendix B):

$$f_{\text{SU}(1,1)}(\Delta\omega) = f(\Delta\omega)(1 + e^{i[(D_s + D_i)L\Delta\omega^2 - \Phi_{\text{ext}}(\Delta\omega)]}). \quad (3)$$

We consider that the experimentally relevant external phase, $\Phi_{\text{ext}}(\Delta\omega)$, consists only of a linear and a quadratic phase. A linear phase can be introduced by a time delay in either one or both of the arms $\Delta t_{s,i}$. The external quadratic phase is realized by placing a dispersive material in the signal or idler arm, which, in addition to a time delay, imprints a quadratic phase characterized by the chirp parameters $C_{s,i}$. The resulting JSA of the full system is presented in

Appendix B. The counts in the signal arm as a function of the delay Δt_s and the external second-order dispersion in the signal and idler arm $C_{s,i}$ can be calculated by integrating over the frequency detuning $\Delta\omega$:

$$\begin{aligned} S(\Delta t_s, \Psi) &= \int_{-\infty}^{\infty} d\Delta\omega |f_{\text{SU}(1,1)}(\Delta\omega)|^2 \\ &= \int_{-\infty}^{\infty} d\Delta\omega \text{sinc}^2(\Delta\gamma\Delta\omega^2)\cos^2(\Psi). \end{aligned} \quad (4)$$

Here, the external second-order dispersion together with the intrinsic waveguide dispersion result in a total phase $\Psi = \frac{1}{2}[\Phi_{\text{ext}} - (D_s + D_i)L\Delta\omega^2]$. Equation (C7) in Appendix C is the final expression that is used to calculate the temporal interferograms presented in this work via numerical integration.

To aid in understanding, an approximate analytical solution can be derived by approximating the sinc^2 term as a

Gaussian, as detailed in Appendix C:

$$S(\Delta t_s, C_s, C_i) \approx \frac{1}{2} + A \exp\left(\frac{\Delta t_s^2}{\sigma_{\text{env}}^2}\right) \times \cos\left(\frac{\zeta \Delta t_s^2}{4\zeta^2 + \Delta \gamma^2} - \bar{\omega}_s \Delta t_s\right). \quad (5)$$

The width of the Gaussian envelope of the temporal interference pattern σ_{env}^2 is given by

$$\sigma_{\text{env}}^2 = \frac{2\zeta}{\Delta \gamma} + 0.5\Delta \gamma, \quad (6)$$

where $\zeta = \Delta \gamma - 0.5(C_s + C_i)$ is the total second-order dispersion in the system. From this expression we can see that the minimal width of the temporal interferogram, i.e., without any second-order dispersion, is given by $0.5\Delta \gamma$ and thereby dependent on the bandwidth of the JSA, as shown in Appendix C. This situation can be reached by cancelation of the intrinsic waveguide dispersion by anomalous external dispersion. For increasing amounts of external chirp $C_{s,i}$, the width of the temporal interferogram increases faster for smaller $\Delta \gamma$. This is because external second-order dispersion leads to a quicker broadening on shorter pulses, a known behavior in classical ultrafast optics. This leads to distinctive behavior for different spectral envelopes of the underlying JSA and thereby correlation times, as schematically shown in Fig. 1(d). This property has been exploited in the following experimental scheme to find the characteristic dependence between the temporal interference width and the second-order dispersion, where we find that not only the spectral bandwidth, but also the spectral shape influences the temporal correlations.

We would like to highlight that our scheme exploits the unique properties of SU(1, 1) interferometers, namely, that the temporal interferogram is sensitive to second-order dispersion. Notably, this effect does not arise in interferometers consisting of linear beam splitters (e.g., Mach-Zehnder interferometer). A study of the sometimes subtle differences between linear and nonlinear interferometers has been published in Ref. [49].

III. EXPERIMENTAL SETUP

The core of the interferometer is a periodically poled Ti:LiNbO₃ guided-wave PDC source with matching signal and idler group velocities, a design that is similarly used in the quantum pulse gate [50]. The use of a waveguide as PDC source generally leads to strong frequency correlations in the JSA, while spatial correlations between the photons do not arise due to generation in single spatial modes. This waveguide is pumped by a 514-nm cw laser, generating PDC light at 830 and 1360 nm in the

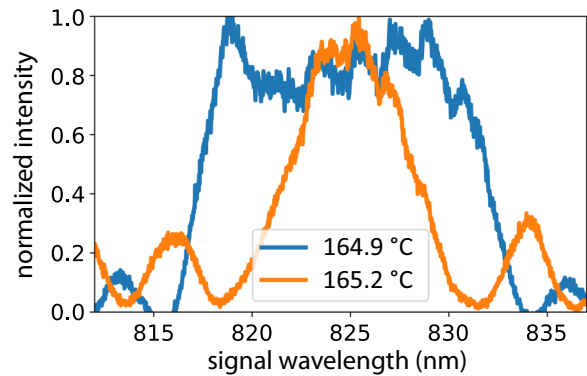


FIG. 2. Measured PDC spectra for temperatures of 164.9 °C (blue) and 165.2 °C (orange) with spectral bandwidths of 6.46 and 2.82 THz. The data are normalized to the maximum intensity of each spectrum and the background of the spectrometer is removed.

signal and idler, respectively. We can reach a spectral bandwidth of more than 6 THz (FWHM) with our 40-mm-long waveguide. The input facet of the waveguide is coated with an antireflection coating for the pump wavelength, while the output facet features a high-reflectivity coating for the pump light to reflect the forward-propagating pump into the reverse direction in the same spatial mode. Both facets are coated with antireflection coatings for the signal and idler wavelengths.

The shape and bandwidth of the emitted PDC spectrum can be tuned by adjusting the waveguide temperature. Different spectral bandwidths then result in different correlation times of the biphoton. We operated our source in a regime with two different spectra, as shown in Fig. 2; cf. Ref. [40]. They cover a spectral bandwidth of 6.46 THz (nominal operating point of the source, blue curve) and 2.82 THz (detuned temperature, orange curve). The temperature difference of the waveguide between these spectra is 0.3 K. Because of the transition from a quasi-top-hat to a sinc² spectral shape, the presented spectra have different time-bandwidth products (TBPs). We calculate them from the FWHM of the simulated spectral and temporal intensities to be around 0.5 and 0.2, respectively, which will be important for the interpretation of our results.

A schematic of the experimental setup is shown in Fig. 3. There, signal and idler photons are generated in the first pass of the pump light through the waveguide and collimated by an off-axis parabolic mirror (OAP). We separate the signal and idler photons using a dichroic mirror. The end mirror of the idler arm can be moved by a motorized stage (PI M111.1DG) to introduce a delay between both arms, resulting in a linear spectral phase. Different amounts of dispersive optical materials can be introduced in one or both of the interferometer arms to imprint a quadratic phase on the biphoton. After reflection on the end mirrors, we couple the signal and idler photons back into the same

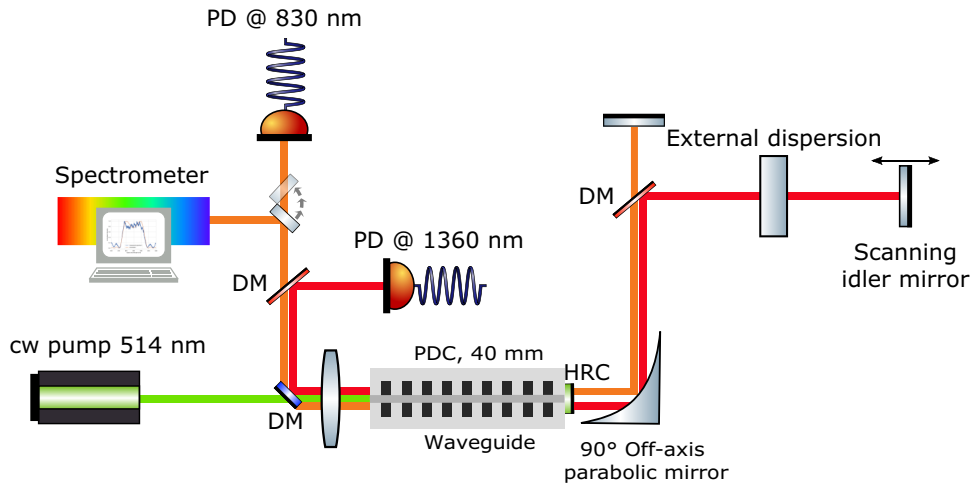


FIG. 3. The experimental setup consisting of a 40-mm-long waveguide as a source for PDC photons in a folded Mach-Zehnder geometry where the pump light is reflected at the waveguide end facet by a high-reflectivity coating (HRC). The setup allows one to add external dispersion in either of the two arms of the interferometer. The end mirror of the idler arm can be moved by a motorized stage. An off-axis parabolic mirror collimates the signal and idler beams and focuses them back into the waveguide. After the second interaction, signal and idler photons are separated from the pump and split up via dichroic mirrors (DMs) and detected by avalanche photodiodes (PDs) or a spectrometer for the signal case.

waveguide via the OAP. The presented design ensures high spectral overlap of the PDC spectra generated in the two processes, as the sources are identical by design.

The fields in the reverse direction are again separated using dichroic mirrors and are detected with a Si avalanche photodiode (APD; Perkin Elmer Photon Counting Module SPCM-AQR-14FC) for the signal light around 830 nm and an (In, Ga)As APD (IDQ id200) for the idler light around 1360 nm for photon counting.

The data from the avalanche photodiodes were recorded with a Swabian Instruments Time-Tagger 20, as the idler mirror was scanned. For each step, the counts were recorded for an integration time of 0.3 s. Without altering the setup, the spectrum of the signal field could be recorded on a single-photon-sensitive spectrometer

(Andor Shamrock SR-500i spectrograph with Newton 970P EMCCD—camera) for a fixed position of the idler mirror. Each spectrum was acquired with an integration time of 1 s and a spectral resolution of about 30 GHz.

IV. RESULTS

The total second-order dispersion is determined by recording spectra of the signal photons for a fixed idler mirror position, resulting in a difference in the interferometers' arm lengths of about 0.3 mm. This allows optimal phase extraction by achieving a balance between maximizing the number of visible interference fringes and ensuring that the measurement is not limited by the resolution of the spectrometer.

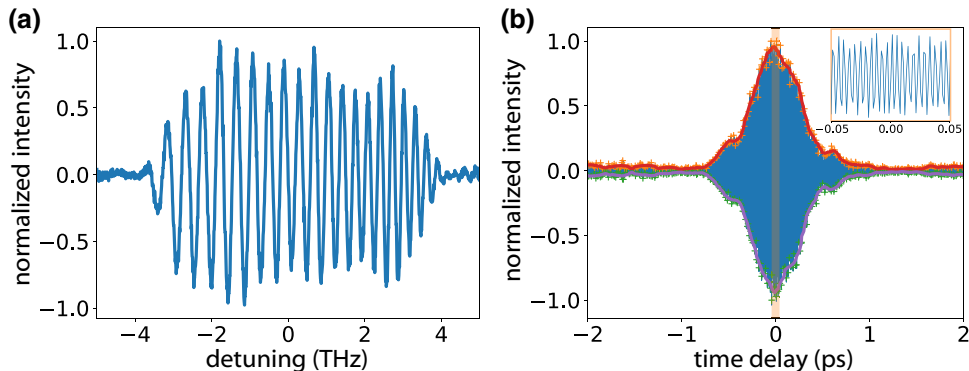


FIG. 4. (a) Spectral interferogram used to extract the second-order dispersion in the system. (b) The corresponding temporal interferogram with upper and lower envelopes, which are used to obtain the temporal interference width. The inset shows an enlarged view of the marked central region of the interferogram.

The second-order dispersion can be estimated by fitting a cosine function to the spectral interferogram. The spectral intensity $S(\Delta\nu)$ with a frequency detuning $\Delta\nu$ around the central frequency is given by [51]

$$S(\Delta\nu) \propto |f'(\Delta\nu)|^2 \{1 + \cos [\Psi(\Delta\nu)]\}. \quad (7)$$

A typical spectral interferogram is shown in Fig. 4(a). This interferogram has been retrieved from the raw data by subtracting a reference spectrum and normalizing the resulting data to their maximum value. The visibility in these interferograms is approximately 30%. A region of 4-THz detuning around the central frequency is used to fit Eq. (7) to ensure a sufficient signal-to-noise ratio for the fit. The uncertainty for the second-order dispersion is given by the fit parameters. We arrive at an intrinsic second-order dispersion for the waveguide itself of about $|\Delta\gamma| = 14\,800 \pm 240$ fs². This value is close to the theoretical value of 10\,893 fs² calculated from the material dispersion of the waveguide. The observed discrepancy can arise from the dielectric end-facet coatings on the waveguide or other elements in the setup, e.g., dichroic mirrors, as well as from imprecisions in the sellmeier model for the refractive index, which is based on an ideal waveguide geometry.

Temporal interferograms were recorded with the same amounts of second-order dispersion added to the interferometer as in the spectral measurements for both PDC spectra. To record the interferogram, the idler mirror was moved over a range of 0.8 mm in steps of 200 nm while recording photon counts at the APDs for signal and idler photons at each step. The inset of Fig. 4(b) shows the interference fringes in the marked central region of the interferogram. The temporal interferograms show visibilities up to 30% for the signal and 15% for the idler, which are each limited by the losses in the other interferometer arm [14,52,53]. To extract the FWHM of the temporal interferogram, the mean number of counts was subtracted from the raw data and the signal was normalized to its maximum value. Furthermore, we fit and smooth the upper and lower envelopes by applying a Savitzky-Golay filter and retrieve the FWHM from the resulting smoothed envelope function; cf. Fig. 4(b). The error on the FWHM of 11.8% is found by measuring the variability within 20 subsequent interferogram measurements with no external dispersion. The resulting relative uncertainty was applied to the other data points. The unprocessed measured spectral and temporal interferograms for these data samples are shown in Appendix E.

The characteristic dependence of the temporal interference width on the total second-order dispersion in the system is revealed by combining temporal and spectral measurements, as shown in Fig. 5. Here, the data points are presented together with simulations of the temporal interference width based on the underlying PDC spectra via

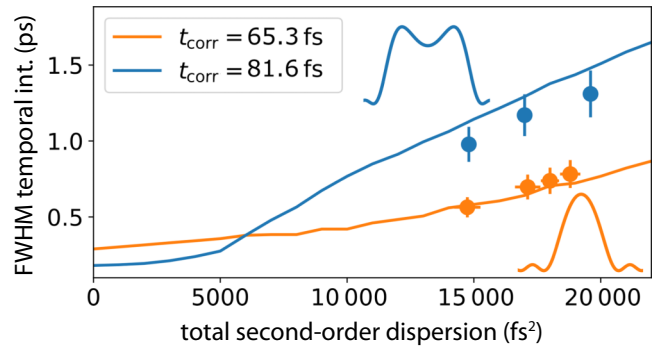


FIG. 5. The change in the temporal interference width with varying second-order dispersion is shown for two different PDC spectra that are depicted in the corresponding color in the figure. The solid lines show simulations based on these spectra.

Eq. (C7) in Appendix C. The spectra are shown schematically in the same color as the corresponding simulation. The simulations reveal a functional dependence between the temporal interference width and second-order dispersion for different shapes of the PDC spectra, as can be seen in Eq. (6). Note that our simulations are based on a parameter-free model that does not take into account deviations from the ideal phase-matching shape or the multimodedeness of the waveguide for the pump and signal fields that lead to deviations from the simulations. During the measurement, alignment of the signal field to the fundamental mode of the waveguide is critical and was seen to be suboptimal at the last data point of the measurement for the broad spectrum. Therefore, this data point has been omitted. Nevertheless, the measured data are in good agreement with the simulations. This allows one to infer the second-order dispersion from the temporal interferogram with no need for single-photon-sensitive spectrometers. The obtained phase information can then be used to calculate the actual correlation time of the generated biphoton by including this phase in the Fourier transform of the JSA.

With this information, the actual correlation times at the output of the PDC source, given as the FWHM of the JTI, can be calculated to be 73.5 and 177.5 fs for the narrower and broader spectra. These actual correlation times are larger than the Fourier-limited ones due to the second-order dispersion of the waveguide material. We can also calculate the minimal correlation time of biphotons via Fourier transform of the two PDC spectra, as stated in Sec. II, assuming a flat phase profile on the JSA. This results in minimal correlation times of 65.3 fs for the narrower spectrum, and 81.6 fs for the broader spectrum. These minimal correlation times can be reached by introducing the correct amount of anomalous second-order dispersion in the setup and would be considered best for experiments requiring high temporal resolution, e.g., entangled two-photon absorption. Note however that

these correlation times vary in a counterintuitive way as the bandwidths vary drastically. This can be attributed to the different TBPs of the different spectral shapes, leading to a shorter correlation time for the narrower spectrum. Furthermore, it should be noted that the exact shape of the temporal interferogram strongly depends on the temporal shape of the biphoton and hence also the criteria for defining the correlation time.

V. CONCLUSION AND OUTLOOK

We have presented a scheme for determining correlation times for a broadband PDC source utilizing an SU(1, 1) interferometer. By performing simultaneous spectral and temporal measurements, we reveal the connection between the second-order dispersion in the system and the FWHM of the temporal interferogram. The data agree with our model for a broadband SU(1, 1) interferometer, where the ideal PDC spectrum is the only free parameter. After validation by the characteristic dependence of the width of the temporal interferogram on the second-order dispersion, the minimal Fourier-limited correlation time could be calculated. For two different underlying PDC spectra, correlation times of 65.3 and 81.6 fs have been extracted. This novel technique can be applied to new emerging integrated sources, e.g., in the field of thin-film lithium niobate, where dispersion engineering plays an even larger role than presented here. It is worth noting that our method is robust against losses between the two PDC stages that only lower the interference visibilities; since the required information is contained in the envelope of the temporal interferogram, established signal processing techniques can be used to overcome low visibilities. Therefore, the measured signal only needs to be distinguishable from noise in the measurement.

The obtained knowledge about the correlation time of the biphoton is important for further experiments, such as entangled two-photon absorption, where the absorption cross section critically depends on the correlation time. Furthermore, the validation of our model enables us to estimate the second-order dispersion of an object under test in the long-wavelength arm by measuring temporal interferograms in the short-wavelength arm, i.e., with undetected photons. Finally, the established connection between spectral and temporal interferograms can be further exploited for source characterization or quantum state manipulation.

ACKNOWLEDGMENTS

F.R. is part of the Max Planck School of Photonics supported by the German Federal Ministry of Education and Research (BMBF), the Max Planck Society, and the Fraunhofer Society. We acknowledge financial support from the Federal Ministry of Education and Research (BMBF) via Grants No. 13N15065 (MiLiQuant) and No. 13N16352 (E2TPA). This project has received funding from the

European Union's Horizon Europe research and innovation programme under Grant Agreement No. 101070700 (MIRAQLS).

APPENDIX A: PDC STATE IN FREQUENCY AND TIME

In the frequency domain, the PDC state can be written as $|\psi\rangle_{\text{PDC}} = \int d\omega_s d\omega_i f(\omega_s, \omega_i) |\omega_s, \omega_i\rangle$ with $|\omega_s, \omega_i\rangle = \hat{a}_s^\dagger(\omega_s) \hat{a}_i^\dagger(\omega_i) |\text{vac}\rangle$ given by the ladder operators in the frequency domain. In the temporal picture, the JSI $\tilde{f}(\tau_s, \tau_i)$ is obtained via two-dimensional Fourier transform of the JSA $f(\omega_s, \omega_i)$ and the ladder operators are transformed via $\tilde{a}(t) = \int d\omega \hat{a}(\omega) e^{-i\omega t}$, leading to $|\tau_s, \tau_i\rangle = \hat{a}_s^\dagger(\tau_s) \hat{a}_i^\dagger(\tau_i) |\text{vac}\rangle$ and finally to the expression of the PDC state in the time domain:

$$|\psi\rangle_{\text{PDC}} = \int d\tau_s d\tau_i \tilde{f}(\tau_s, \tau_i) |\tau_s, \tau_i\rangle. \quad (\text{A1})$$

A more detailed description can be found in Ref. [28].

APPENDIX B: TAYLOR EXPANSION OF THE PHASE MISMATCH

We start by performing the Taylor expansion of the phase mismatch $\Delta\beta$ for the specific case of pumping the PDC with a cw laser. The full expression, already written in terms of the frequency detuning $\Delta\omega = \omega_s - \bar{\omega}_s = -(\omega_i - \bar{\omega}_i)$, takes the form

$$\begin{aligned} \Delta\beta(\omega_s, \omega_i) &= k_p(\omega_s + \omega_i) - k_s(\omega_s) - k_i(\omega_i) \\ &= \Delta\beta^{(0)} + (\kappa_s - \kappa_i)\Delta\omega + (\eta_s + \eta_i)\Delta\omega^2 \\ &\quad + \eta_p\Delta\omega(-\Delta\omega). \end{aligned} \quad (\text{B1})$$

Here, we assume that $\Delta\beta^{(0)}$ can be set to zero by periodic poling. To obtain the negative sign in the last term, we made use of the fact that $\Delta\omega = (\omega_s - \bar{\omega}_s) = -(\omega_i - \bar{\omega}_i)$ due to the strong frequency correlations in the case of cw pumping. In the above expression, $\kappa_s = L[(\partial k_p / \partial \omega)|_{\bar{\omega}_s + \bar{\omega}_i} - (\partial k_s / \partial \omega)|_{\bar{\omega}_s}]$ and analogously for κ_i , $\eta_s = (L/2)[(\partial^2 k_p / \partial \omega^2)|_{\bar{\omega}_s + \bar{\omega}_i} - (\partial^2 k_s / \partial \omega^2)|_{\bar{\omega}_s}]$ and analogously for η_i , and, lastly, $\eta_p = L(\partial^2 k_p / \partial \omega^2)|_{\bar{\omega}_s + \bar{\omega}_i}$. We see that terms containing $\partial k_p / \partial \omega$ and $\partial^2 k_p / \partial \omega^2$ are canceled out as we consider the specific case of cw pumping.

We now take a closer look at the resulting expression for $\Delta\beta$ in the case of cw pumping expanded to second order:

$$\begin{aligned} \Delta\beta(\Delta\omega) &\approx -\left.\frac{\partial k_s}{\partial \omega}\right|_{\bar{\omega}_s} \Delta\omega + \left.\frac{\partial k_i}{\partial \omega}\right|_{\bar{\omega}_i} \Delta\omega \\ &\quad - \left.\frac{\partial^2 k_s}{\partial \omega^2}\right|_{\bar{\omega}_s} \Delta\omega^2 - \left.\frac{\partial^2 k_i}{\partial \omega^2}\right|_{\bar{\omega}_i} \Delta\omega^2 \end{aligned} \quad (\text{B2})$$

with $(\partial k_s / \partial \omega)|_{\bar{\omega}_s} = 1/v_{g,s}$ and $(\partial k_i / \partial \omega)|_{\bar{\omega}_i} = 1/v_{g,i}$ the inverse signal and idler group velocities, respectively. The

second-order derivatives are connected to the group velocity dispersion of the signal and idler fields by $D_{s,i} = (\partial^2 k_{s,i}/\partial \omega^2)|_{\bar{\omega}_{s,i}}$.

We can see that a broad PDC spectrum can be achieved by group-velocity matching, which requires tailoring the dispersion in a way that $v_{g,s} = v_{g,i}$. This leads to a phase mismatch $\Delta\beta$ that now only shows a quadratic term at leading order:

$$\Delta\beta(\omega_s, \omega_i) \approx -\frac{\partial^2 k_s}{\partial \omega^2}\Big|_{\bar{\omega}_s} \Delta\omega^2 - \frac{\partial^2 k_i}{\partial \omega^2}\Big|_{\bar{\omega}_i} \Delta\omega^2. \quad (\text{B3})$$

APPENDIX C: SU (1, 1) JOINT SPECTRAL AMPLITUDE

To construct the joint spectral amplitude at the output of the SU(1, 1) interferometer, i.e., after going through the second PDC process, we consider the two individual amplitudes first and sum them up afterwards.

The photons produced in the first pass of the pump field through the PDC source experience the second-order dispersion introduced in either of the interferometer arms as well as dispersion from the waveguide material itself, during the generation process and when passing through the waveguide for the second time. We assume that no nonlinear process occurs during that second pass, such that the generated photons only propagate through the waveguide, but do not interact with the pump field.

An external phase, e.g., second-order dispersion, on the joint spectral amplitude of a single PDC source can be described by [28]

$$f_{\text{phase}}(\Delta\omega) = f(\Delta\omega)E(\Delta\omega), \quad (\text{C1})$$

where $f(\Delta\omega)$ is the JSA of a single PDC source and $E(\Delta\omega) = \exp[\Psi]$ includes the total phase Ψ accumulated by the PDC from the first pass. Therefore, we can write this JSA as

$$f_1(\Delta\omega) = f(\Delta\omega)\exp[-i(D_s L + C_s)\Delta\omega^2 + \omega_s \Delta t_s] \times \exp[-i(D_i L + C_i)\Delta\omega^2], \quad (\text{C2})$$

where $D_{s,i}$ and $C_{s,i}$ are the second-order dispersion of the waveguide and the external second-order dispersion on the signal and idler, respectively, and Δt_s is a time delay added to the signal arm.

The photons generated during the second pass of the pump field do not propagate through the interferometer arms and thus only acquire the phase included in the JSA of a single PDC source $f_2(\Delta\omega) = f(\Delta\omega)$. This results in the total JSA given by

$$f_{\text{SU}(1,1)}(\Delta\omega) = f_1(\Delta\omega) + f_2(\Delta\omega) = f(\Delta\omega)(1 + e^{-i(D_s L + D_i L + C_s + C_i)\Delta\omega^2 - i\omega_s \Delta t_s}). \quad (\text{C3})$$

It can be seen directly from this expression that, due to the lack of cross-terms, the quadratic phase in either of the arms can be compensated by placing the corresponding amount of dispersion in either the same or the other arm of the interferometer [54].

The external phase can be rewritten as

$$\begin{aligned} \Phi_{\text{ext}}(\Delta\omega) &= \omega_s \Delta t_s + C_s \Delta\omega^2 + C_i \Delta\omega^2 \\ &= (\bar{\omega}_s + \Delta\omega) \Delta t_s + C_s \Delta\omega^2 + C_i \Delta\omega^2. \end{aligned} \quad (\text{C4})$$

This leads to an expression for the total phase of

$$\Psi = \frac{1}{2}\{[(D_s + D_i)L - C_s - C_i]\Delta\omega^2 - \Delta t_s \bar{\omega}_s - \Delta t_s \Delta\omega\}. \quad (\text{C5})$$

When expressing the real part of the exponential function as a cosine function, the total JSA becomes

$$f_{\text{SU}(1,1)}(\Delta\omega, C_s, C_i, \Delta t_s) = 2f(\Delta\omega) \cos(\Psi) \exp\left(i\frac{\Psi}{2}\right). \quad (\text{C6})$$

The resulting single-photon counts, forming the temporal interferogram, are then given by integration:

$$\begin{aligned} S(\Delta t_s, \Psi) &= \int_{-\infty}^{\infty} d\Delta s \omega |f_{\text{SU}(1,1)}(\Delta\omega)|^2 \\ &= \int_{-\infty}^{\infty} d\Delta\omega \text{sinc}^2(\Delta\gamma \Delta\omega^2) \cos^2(\Psi). \end{aligned} \quad (\text{C7})$$

APPENDIX D: ANALYTICAL APPROXIMATE SOLUTION

To find an approximate analytical solution, we split the cosine term in Eq. (C7) into three terms,

$$\cos^2(\Psi) = \frac{1}{2} + \frac{1}{4}e^{2i\Psi} + \frac{1}{4}e^{-2i\Psi}, \quad (\text{D1})$$

such that $S(\Delta t_s, \Psi) = I_1 + I_2 + I_3$. Furthermore, the sinc^2 term can be approximated by a Gaussian function in the latter two integrals:

$$\text{sinc}^2(\Delta\gamma \Delta\omega^2) \approx \exp\left(-\frac{\Delta\gamma}{\sigma} \Delta\omega^2\right) \quad (\text{D2})$$

with $\Delta\gamma = -(D_s + D_i)L/2$ and $\sigma = 2$ to match the FWHM of both functions. The first integral yields a constant offset of 0.5, as the result of an integral of a Gaussian.

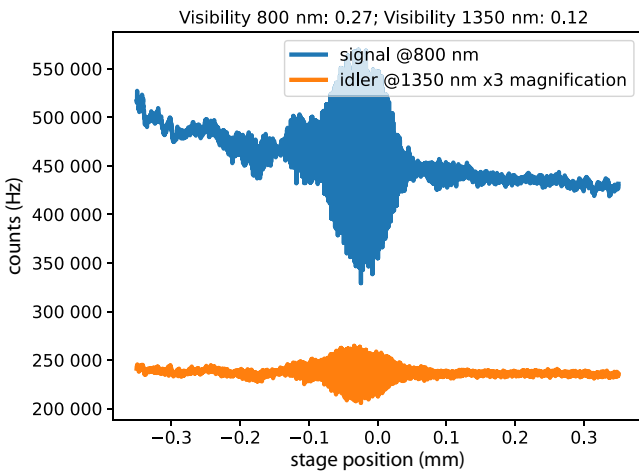


FIG. 6. The measured counts of signal and idler photons at the output of the interferometer for different idler stage positions. The counts in the idler arm have been multiplied by a factor of 3.

With the approximation, I_2 becomes

$$I_2 = A \exp(-i\bar{\omega}_s \Delta t_s) \\ \times \exp\left(\frac{\Delta t_s^2 [i\Delta\gamma - 0.5i(C_s + C_i) + 0.5\Delta\gamma]}{\Delta\gamma + 2[\Delta\gamma - 0.5(C_s + C_i)]^2}\right), \quad (\text{D3})$$

where $A = 2/(3|\Delta\gamma|^{1/2} \sqrt{-\Delta\gamma + C_s + C_i})$. Integral I_3 yields the complex conjugate of I_2 . We can identify $\zeta = \Delta\gamma - 0.5(C_s + C_i)$ as the total second-order dispersion in the system. Put together, this results in a temporal interferogram given by

$$S(\Delta t_s, C_s, C_i) = \frac{1}{2} + A \exp\left(\frac{\Delta\gamma \Delta t_s^2}{2\zeta^2 + 0.5\Delta\gamma^2}\right) \\ \times \cos\left(\frac{\zeta \Delta t_s^2}{4\zeta^2 + \Delta\gamma^2} - \bar{\omega}_s \Delta t_s\right). \quad (\text{D4})$$

The frequency of the interference fringes is mainly given by the central frequency of the light in signal arm $\bar{\omega}_s$, but also slightly influenced by the second-order phase in the interferometer, which causes a relative time delay of different frequencies. The prefactor A determines the visibility of the interference pattern, which also depends on internal and externally applied second-order dispersion. It becomes apparent that the width of the envelope of the temporal interferogram is given by the intrinsic second-order dispersion of the nonlinear material, represented by parameter $\Delta\gamma$, and can be altered by adding dispersive elements in the signal or idler arm introducing C_s and C_i . It is thereby irrelevant how the second-order phase is distributed between the photons, an effect that is also known as nonlocal dispersion cancellation [54].

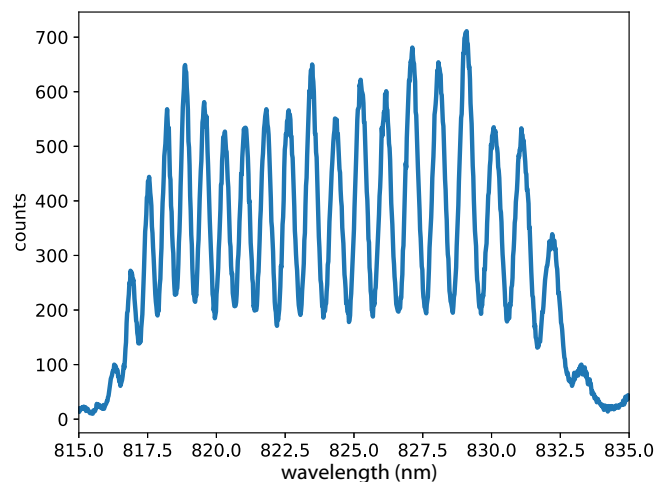


FIG. 7. The measured signal spectrum showing interference. The background counts of the camera have been subtracted from the spectrum.

APPENDIX E: EXAMPLE OF UNPROCESSED SPECTRAL AND TEMPORAL INTERFEROGRAMS

An unprocessed temporal interferogram containing signal and idler counts, where the idler counts have been multiplied by a factor of 3 for better display, for different stage positions is shown in Fig. 6. An unprocessed spectral interferogram, measured at a fixed delay from the signal output of the interferometer is presented in Fig. 7.

- [1] S. Mukamel, *et al.*, Roadmap on quantum light spectroscopy, *J. Phys. B: At., Mol. Opt. Phys.* **53**, 072002 (2020).
- [2] B. Brecht, D. V. Reddy, C. Silberhorn, and M. G. Raymer, Photon temporal modes: A complete framework for quantum information science, *Phys. Rev. X* **5**, 041017 (2015).
- [3] K. E. Dorfman, F. Schlawin, and S. Mukamel, Nonlinear optical signals and spectroscopy with quantum light, *Rev. Mod. Phys.* **88**, 045008 (2016).
- [4] A. Pe'er, B. Dayan, A. A. Friesem, and Y. Silberberg, Temporal shaping of entangled photons, *Phys. Rev. Lett.* **94**, 073601 (2005).
- [5] B. Dayan, A. Pe'er, A. A. Friesem, and Y. Silberberg, Nonlinear interactions with an ultrahigh flux of broadband entangled photons, *Phys. Rev. Lett.* **94**, 043602 (2005).
- [6] Z. Zhang, T. Peng, X. Nie, G. S. Agarwal, and M. O. Scully, Entangled photons enabled time-frequency-resolved coherent Raman spectroscopy and applications to electronic coherences at femtosecond scale, *Light Sci. Appl.* **11**, 274 (2022).
- [7] D. J. Kane and R. Trebino, Single-shot measurement of the intensity and phase of an arbitrary ultrashort pulse by using frequency-resolved optical gating, *Opt. Lett.* **18**, 823 (1993).

- [8] C. Iaconis and I. A. Walmsley, Spectral phase interferometry for direct electric-field reconstruction of ultrashort optical pulses, *Opt. Lett.* **23**, 792 (1998).
- [9] B. Yurke, S. L. McCall, and J. R. Klauder, SU(2) and SU(1,1) interferometers, *Phys. Rev. A* **33**, 4033 (1986).
- [10] M. V. Chekhova and Z. Y. Ou, Nonlinear interferometers in quantum optics, *Adv. Opt. Photonics* **8**, 104 (2016).
- [11] D. Li, C.-H. Yuan, Z. Y. Ou, and W. Zhang, The phase sensitivity of an SU(1,1) interferometer with coherent and squeezed-vacuum light, *New J. Phys.* **16**, 073020 (2014).
- [12] Y. Shaked, Y. Michael, R. Vered, L. Bello, M. Rosenbluh, and A. Pe'er, Lifting the bandwidth limit of optical homodyne measurement with broadband parametric amplification, *Nat. Commun.* **9**, 609 (2018).
- [13] M. Manceau, G. Leuchs, F. Khalili, and M. Chekhova, Detection loss tolerant supersensitive phase measurement with an SU(1,1) interferometer, *Phys. Rev. Lett.* **119**, 223604 (2017).
- [14] M. Santandrea, K.-H. Luo, M. Stefszky, J. Sperling, H. Herrmann, B. Brecht, and C. Silberhorn, Lossy SU(1,1) interferometers in the single-photon-pair regime, *Quantum Sci. Technol.* **8**, 025020 (2023).
- [15] J. Flórez, E. Pearce, N. R. Gemmell, Y. Ma, G. Bressanini, C. C. Phillips, R. F. Oulton, and A. S. Clark, Enhanced nonlinear interferometry via seeding, *ArXiv:2209.06749*.
- [16] D. Kalashnikov, A. Paterova, and S. Kulik, Infrared spectroscopy with visible light, *Nat. Photonics* **10**, 98 (2016).
- [17] L. Cui, J. Su, J. Li, Y. Liu, X. Li, and Z. Y. Ou, Quantum state engineering by nonlinear quantum interference, *Phys. Rev. A* **102**, 033718 (2020).
- [18] J. Su, L. Cui, J. Li, Y. Liu, X. Li, and Z. Y. Ou, Versatile and precise quantum state engineering by using nonlinear interferometers, *Opt. Express* **27**, 20479 (2019).
- [19] G. B. Lemos, V. Borish, G. D. Cole, S. Ramelow, R. Lapkiewicz, and A. Zeilinger, Quantum imaging with undetected photons, *Nature* **512**, 409 (2014).
- [20] C. Lindner, J. Kunz, S. J. Herr, S. Wolf, J. Kießling, and F. Kühnemann, Nonlinear interferometer for Fourier-transform mid-infrared gas spectroscopy using near-infrared detection, *Opt. Express* **29**, 4035 (2021).
- [21] S. Töpfer, M. G. Basset, J. Fuenzalida, F. Steinlechner, J. P. Torres, and M. Gräfe, Quantum holography with undetected light, *Sci. Adv.* **8**, eabd4301 (2022).
- [22] A. Paterova, H. Yang, C. An, D. Kalashnikov, and L. Krivitsky, Measurement of infrared optical constants with visible photons, *New J. Phys.* **20**, 043015 (2018).
- [23] P. Kaufmann, H. M. Chrzanowski, A. Vanselow, and S. Ramelow, Mid-IR spectroscopy with NIR grating spectrometers, *Opt. Express* **30**, 5926 (2022).
- [24] I. Kviatkovsky, H. M. Chrzanowski, E. G. Avery, H. Bartolomaeus, and S. Ramelow, Microscopy with undetected photons in the mid-infrared, *Sci. Adv.* **6**, eabd0264 (2020).
- [25] A. Rojas-Santana, G. J. Machado, M. V. Chekhova, D. Lopez-Mago, and J. P. Torres, Analysis of the signal measured in spectral-domain optical coherence tomography based on nonlinear interferometers, *Phys. Rev. A* **106**, 033702 (2022).
- [26] A. Vallés, G. Jiménez, L. J. Salazar-Serrano, and J. P. Torres, Optical sectioning in induced coherence tomography with frequency-entangled photons, *Phys. Rev. A* **97**, 023824 (2018).
- [27] T. Tashima, Y. Mukai, M. Arahata, N. Oda, M. Hisamitsu, K. Tokuda, R. Okamoto, and S. Takeuchi, Ultra-broadband quantum infrared spectroscopy, *Optica* **11**, 81 (2024).
- [28] Y. Jeronimo-Moreno and A. B. U'Ren, Control, measurement, and propagation of entanglement in photon pairs generated through type-II parametric down-conversion, *Phys. Rev. A* **79**, 033839 (2009).
- [29] S.-Y. Baek, O. Kwon, and Y.-H. Kim, Nonlocal dispersion control of a single-photon waveform, *Phys. Rev. A* **78**, 013816 (2008).
- [30] S.-Y. Baek, O. Kwon, and Y.-H. Kim, Temporal shaping of a heralded single-photon wave packet, *Phys. Rev. A* **77**, 013829 (2008).
- [31] A. Valencia, M. V. Chekhova, A. Trifonov, and Y. Shih, Entangled two-photon wave packet in a dispersive medium, *Phys. Rev. Lett.* **88**, 183601 (2002).
- [32] S. E. Harris, Chirp and compress: Toward single-cycle biphotons, *Phys. Rev. Lett.* **98**, 063602 (2007).
- [33] Y. Shaked, R. Pomerantz, R. Z. Vered, and A. Pe'er, Observing the nonclassical nature of ultra-broadband biphotons at ultrafast speed, *New J. Phys.* **16**, 053012 (2014).
- [34] Y. Shaked, S. Yefet, T. Geller, and A. Pe'er, Octave-spanning spectral phase control for single-cycle bi-photons, *New J. Phys.* **17**, 073024 (2015).
- [35] C. K. Hong, Z. Y. Ou, and L. Mandel, Measurement of subpicosecond time intervals between two photons by interference, *Phys. Rev. Lett.* **59**, 2044 (1987).
- [36] Y.-R. Fan, C.-Z. Yuan, R.-M. Zhang, S. Shen, P. Wu, H.-Q. Wang, H. Li, G.-W. Deng, H.-Z. Song, L.-X. You, Z. Wang, Y. Wang, G.-C. Guo, and Q. Zhou, Effect of dispersion on indistinguishability between single-photon wave-packets, *Photonics Res.* **9**, 1134 (2021).
- [37] W. Zhao, N. Huo, L. Cui, X. Li, and Z. Y. Ou, Propagation of temporal mode multiplexed optical fields in fibers: Influence of dispersion, *Opt. Express* **30**, 447 (2022).
- [38] D.-G. Im, Y. Kim, and Y.-H. Kim, Dispersion cancellation in a quantum interferometer with independent single photons, *Opt. Express* **29**, 2348 (2021).
- [39] J.-P. W. MacLean, J. M. Donohue, and K. J. Resch, Ultra-fast quantum interferometry with energy-time entangled photons, *Phys. Rev. A* **97**, 063826 (2018).
- [40] R. Pollmann, F. Roeder, V. Quiring, R. Ricken, C. Eigner, B. Brecht, and C. Silberhorn, Integrated, bright, broadband parametric down-conversion source for quantum metrology and spectroscopy, *ArXiv:2402.17515*.
- [41] Aron Vanselow, Paul Kaufmann, Helen M. Chrzanowski, and Sven Ramelow, Ultra-broadband SPDC for spectrally far separated photon pairs, *Opt. Lett.* **44**, 4638 (2019).
- [42] J. Williams, R. Nehra, E. Sendonaris, L. Ledezma, R. M. Gray, R. Sekine, and A. Marandi, Ultra-short pulse biphoton source in lithium niobate nanophotonics at 2 μm , *ArXiv:2402.05163*.
- [43] M. Jankowski, J. Mishra, and M. M. Fejer, Dispersion-engineered $\chi^{(2)}$ nanophotonics: A flexible tool for nonclassical light, *J. Phys.: Photonics* **3**, 042005 (2021).

- [44] W. P. Grice and I. A. Walmsley, Spectral information and distinguishability in type-II down-conversion with a broadband pump, *Phys. Rev. A* **56**, 1627 (1997).
- [45] C. K. Law, I. A. Walmsley, and J. H. Eberly, Continuous frequency entanglement: Effective finite Hilbert space and entropy control, *Phys. Rev. Lett.* **84**, 5304 (2000).
- [46] M. Avenhaus, A. Eckstein, P. J. Mosley, and C. Silberhorn, Fiber-assisted single-photon spectrograph, *Opt. Lett.* **34**, 2873 (2009).
- [47] O. Kuzucu, F. N. C. Wong, S. Kurimura, and S. Tovstonog, Joint temporal density measurements for two-photon state characterization, *Phys. Rev. Lett.* **101**, 153602 (2008).
- [48] A. B. U'Ren, C. Silberhorn, K. Banaszek, I. Walmsley, R. Erdmann, W. Grice, and M. G. Raymer, Generation of pure-state single-photon wavepackets by conditional preparation based on spontaneous parametric downconversion, *Laser Phys.* **15**, 146 (2005).
- [49] K.-H. Luo, M. Santandrea, M. Stefszky, J. Sperling, M. Massaro, A. Ferreri, P. R. Sharapova, H. Herrmann, and C. Silberhorn, Quantum optical coherence: From linear to nonlinear interferometers, *Phys. Rev. A* **104**, 043707 (2021).
- [50] A. Eckstein, B. Brecht, and C. Silberhorn, A quantum pulse gate based on spectrally engineered sum frequency generation, *Opt. Express* **19**, 13770 (2011).
- [51] A. Riazi, E. Y. Zhu, C. Chen, A. V. Gladyshev, P. G. Kazansky, and L. Qian, Alignment-free dispersion measurement with interfering biphotons, *Opt. Lett.* **44**, 1484 (2019).
- [52] Y. Michael, I. Jonas, L. Bello, M.-E. Meller, E. Cohen, M. Rosenbluh, and A. Pe'er, Augmenting the sensing performance of entangled photon pairs through asymmetry, *Phys. Rev. Lett.* **127**, 173603 (2021).
- [53] N. R. Gemmell, J. Flórez, E. Pearce, O. Czerwinski, C. C. Phillips, R. F. Oulton, and A. S. Clark, Loss-compensated and enhanced midinfrared interaction-free sensing with undetected photons, *Phys. Rev. Appl.* **19**, 054019 (2023).
- [54] J. D. Franson, Nonlocal cancellation of dispersion, *Phys. Rev. A* **45**, 3126 (1992).